CYCLIC LOW-THERMAL AGING OF DISSIMILAR AUSTENITIC STEEL WELDS USED IN NUCLEAR POWER PLANTS

JAN HRACEK[1], HANA SEBESTOVA[2], SARKA MIKMEKOVA[2], ONDREJ AMBROZ[2], LIBOR MRNA[2]

[1]Faculty of Mechanical Engineering, Brno University of Technology, Brno, Czech Republic

[2]Institute of Scientific Instruments of the Czech Academy of Sciences, Brno, Czech Republic

DOI: 10.17973/MMSJ.2024_12_2024046

sebestova@isibrno.cz

The nuclear power plants in Eastern Europe face problems with supplies of spare parts manufactured according to the same Russian standards as the originals. Therefore, the dissimilar welds of original Russian steel 08Ch18N10T and substitutive 1.4541 were made and analyzed to consider the possibility of original steel replacement during the repairs. Two different filler wires were applied. The welds were subjected to cyclic thermal loading corresponding to the actual operating conditions of a nuclear unit, and their microstructure and mechanical properties were compared to the as-welded joints. An increase in weld metal microhardness induced by aging was found when the filler with higher C and Cr content was used. Although this could indicate possible ferrite decomposition, the detected changes in mechanical properties corresponded to the changes in homogeneous welds of the original steel. The strength requirements for the steel used in nuclear power plant devices were still matched.

KEYWORDS

dissimilar weld, austenitic steel, thermal aging, replacement, microstructure, mechanical properties, nuclear power plant

1 INTRODUCTION

Nowadays, Czech and other nuclear power plants (NPPs) of the water-water energetic reactor (WWER) of the USSR construction built in countries of Eastern Europe use the material for equipment, pipes, and construction in the primary circuit manufactured according to Russian directives such as the national standard called GOST. Since the collapse of the Eastern bloc, these NPPs have had issues with supplies of tubes, filler welding materials, and others in small amounts for repairs and maintenance. Therefore, substitutive steels had to be introduced to replace the original Russian steel.

All materials used to manufacture NPPs should be certified under Normative technical documentation of the Association of Mechanical Engineers (NTD AME) [Kander 2023] requirements for the Czech Republic or PNAE G-7-002-86 [Energoatomizdat 1987] for other locations. The original Russian austenitic stainless steel grade 08Ch18N10T is used in the primary circuit because of its high corrosion resistance, excellent weldability, and good mechanical properties. The mechanical properties of 08Ch18N10T are summarized in Tab. 1. Tab. 2 presents its chemical composition according to the GOST 5632 standard [GOST 2014].

Standard	$R_{p0.2}$ (MPa)	R_m (MPa)	A (%)
NTD AME	216	510	35
PNAE G-7-002-86	196	491	38

Table 1. Yield strength ($R_{p0.2}$), ultimate tensile strength (R_m), and total elongation (A) of 08Ch18N10T according to different standards

C	Cr	Ni	Si	Mn
< 0.08	17–19	9–11	< 0.08	< 2
Ti	**S**	**P**	**Fe**	
< 0.7 (5×C)	< 0.02	< 0.04	Bal.	

Table 2. Chemical composition of 08Ch18N10T in wt. % according to the GOST 5632 standard.

The choice of material for component fabrication, repair, or refurbishment of NPP equipment takes into account the chemical composition, physical and mechanical properties, weldability, and suitability for use under the operating conditions (12.25 MPa, 322 °C) of the equipment throughout its expected lifetime.

In addition to physical and mechanical properties, the cobalt content of material for equipment operating in the primary circuit of NPP is also controlled because it can become a radiator at electron fluence F > 10^{22} nm^{-2} with energy > 0.5 MeV. Such a component is then dangerous for both the operator and the equipment maintainer. For the austenitic steels, cobalt content up to 0.050 wt.% is permissible.

Ti-stabilized austenitic stainless steel weld metal (WM) contains the δ ferrite that might be unstable at long-term exposure to increased temperatures. The spinodal decomposition of ferrite forms Fe-rich and Cr-rich regions below 500 °C, while temperatures above 550 °C promote the formation of the σ phase [Subramanian 2018]. The σ phase is a brittle Cr-rich intermetallic phase with a tetragonal body-centered crystal structure. Its precipitation temperature depends on the chemical composition of the alloy [Hsieh 2012]. The σ phase can increase the hardness and decrease the toughness and elongation of steel [Lee 2003].

According to the Schaeffler diagram adopted for weldability prediction, the σ phase can precipitate in the stainless steels with the chromium equivalent > 23 [Brandi 2017]. The precipitation of the σ phase is not readily observable in austenitic stainless steels with Cr content below 20 % [Peckner 1977]. Several empiric equations for σ phase prediction were referred [Hsieh 2012]. According to [Gow 1942], the σ phase could precipitate in the stainless steel when the ratio factor calculated as (%Cr-16%C)/%Ni exceeds 1.7. Based on Tab. 2, the ratio factor of the 08Ch18N10T steel can be 1.4–2.0. Therefore, forming the σ phase in this steel is possible. However, the predictions of the σ phase based on the empirical formulas might be inadequate since this type of problem is markedly nonlinear [Brandi 2017].

Typically, 1.4541 steel is a new substitute for the original Russian steel 08Ch18N10T. Other grades of austenitic stainless steel, like 316L, 321, or 1.4571, are also allowed by NTD AME to be used in NPP. However, they can be sensitive to grain coarsening of the heat-affected zone (HAZ) exposed to temperatures above about 1400 °C [Eghlimi 2015, Fujiyama 2018]. It can be avoided using lower heat input welding technology [Klimpel 2007, Lapsanska 2010].

The decreased content of Ni in these steels is supposed to promote a higher portion of δ ferrite in the WM. The ferrite reduces weld susceptibility to hot cracking. Therefore, despite the risk of ferrite decomposition during thermal aging, austenitic steels with a small content of δ ferrite are used in NPP applications. The possible microstructural changes during the service are often overlooked during the design of components other than the pressure vessel of a reactor, e.g., pipelines.

Ferrite also increases fatigue resistance compared to fully austenitic microstructure. However, thermal aging of δ ferrite-containing material results in a significant reduction in fatigue resistance [Wang 2022]. The degradation of mechanical properties is proportional to the amount of σ phase being precipitated [Chen 2002]. The σ phase also worsens the corrosion resistance because the surrounding zones are Cr-depleted [Nagae 2022]. Although the NTD AME does not prescribe the tests of welds, all these aspects must be considered when choosing the substitutive material for the repairs or replacements of components operating in NPPs, especially the dissimilar welds need to be investigated in detail.

Kumar et al. [Kumar 2021] investigated the deformation failure behavior of welds of austenitic 316 LN stainless steel grades under thermo-mechanical low-cycle fatigue. The cyclic loading led to weld strengthening, hardness dispersion reduction, and σ phase initiation. However, thermal aging increased the fatigue life of welded samples.

Dutt et al. [Dutt 2011] evaluated the mechanical behavior of 316L (N) welds after long-term exposure (20,000 h) to service temperatures at 370, 475 and 550 °C. A general decrease in resistance to crack initiation was observed for all aged welds. The Charpy energy of specimens subjected to aging at 475 °C decreased. Changes in tensile properties were negligible. The embrittlement is due to the formation of new phases in δ ferrite regions. The α-α′ spinodal decomposition is predominant at lower temperatures (370 °C and 475 °C), causing strain inhomogeneities leading to a reduction in toughness, while σ phase formation is essential at 550 °C.

The effect of thermal aging of 316 L austenitic stainless steel TIG welds made with ER316L filler was evaluated in [Jeong 2022]. The separation of Fe-rich and Cr-rich phases was observed in the samples aged at 400 °C for 5,000 h. It led to about 13-20% increase in ultimate tensile strength (UTS). Chandra et al. [Chandra 2012] investigated low-thermal aging of 304L and 316L austenitic steel welds. Thermal aging at 400 °C led to spinodal decomposition and G-phase precipitation in the ferrite phase. The ferrite microhardness was almost doubled after 10,000 h of aging at 400 °C. The aging up to 20,000 h at 335 °C and 365 °C showed only a spinodal decomposition, causing a lower increase in ferrite microhardness.

Both [Chandra 2012] and [Jeong 2022] concluded that the formation of phases causing embrittlement of austenitic steel welds containing δ ferrite occurs during the aging close to the operating temperatures of Pressurized Water Reactor (PWR) type reactors similar to WWER type. To justify the possibility of prolonging the service life of NPPs type WWER, the effect of thermal aging on the mechanical properties of 08Ch18N10T stainless steel was intensively studied in the Russian Federation in the first decade of the new millennium. However, not much research has been published. In the technical report [Kazantsev 2009], the mechanical properties of the piping of the pressurizer system that has been operating for 30 years were evaluated. Both the 08Ch18N10T base metal (BM) and the welds were considered to still safely fulfill prescribed standards. Then, the additional thermal aging at 450 °C for 1300 h, simulating another possible 30 years of service, was applied. The UTS values of both the BM and welds after this additional aging increased by less than 4 % towards the samples after 30 years of service. Their impact strength at room temperature increased by 15 % which is in an acceptable range.

However, the NPP piping components must withstand rather a short time exposure to increased temperatures, but repeatedly. Temperature changes occur during the planned NPP outage due to fuel exchange and the NPP subsequent return to service. Rapid temperature changes also arise during normal cyclic operations corresponding to the need for primary circuit cooling medium release, e.g. in the main safety valve system that is not heated up to maximum operation temperature during casual operation.

In this paper, we analyze the dissimilar welds combining original 08Ch18N10T and substitutive 1.4541 steel, which is unusual. The 1.4541 steel reaches the ratio factor of 1.74 and the used filler wires 1.8–1.9. Thus, the presence of ferrite in the WM is expected, and the risk that it can promote the formation of σ phase at high temperatures during the cooling of a weld should be explored. The welds were further subjected to cyclic thermal loading corresponding to the real operating conditions of a nuclear unit. The 150 cycles with maximal temperature of 300 °C were applied, and the microstructure and mechanical properties of aged welds were compared to those of the as-welded joints to evaluate possible degradation. To our knowledge, such research on dissimilar weld joints combining original and substitutive steel has not been published.

2 MATERIALS AND METHODS

The standard grade of Russian steel 08Ch18N10T as an original and 1.4541 steel grade as a substitute were chosen for the experiment. The dissimilar weld made with the filler wire Sv-04Ch19N11M3 was assigned as sample A and the wire Sv-08Ch19N10 G2B was used for sample B. These original Russian filler welding materials are used for repair welding in the primary circuit. The chemical composition of steels and filler welding materials used in the experiment are listed in Tab. 3.

All these materials should have an austenitic matrix with the amount of δ ferrite listed in Tab. 4. The ferrite content declared by the inspection certificate was measured with Fischer Feritscope FC-2 according to GOST 246-70 standard.

The mechanical properties of experimental BMs and fillers are concluded in Tab. 5.

Material	C	Cr	Ni	Ti	Mn	Si	P	S	Cu	Mo	V	N	Co	Nb	Fe
08Ch18N10T	0.062	17.35	10.85	0.52	1.36	0.42	0.021	0.001	0.17	0.2	0.04	0.014	0.04	0	Bal.
1.4541	0.06	17.30	9.39	0.53	1.45	0.27	0.031	0.011	0	0	0	0	0	0	Bal.
Sv-04Ch19N11M3	0.017	18.22	10.00	0	1.91	0.34	0.016	0.013	0	2.13	0	0	0.025	0	Bal.
Sv-08Ch19N10G2B	0.05	19.34	9.94	0	1.92	0.44	0.015	0.002	0	0	0	0	0.036	1.28	Bal.

Table 3. Chemical composition of used base and filler materials (wt. %)

Material	Estimated based on the Schaeffler diagram	Declared by the inspection certificate
08Ch18N10T	0	2.1
1.4541	2	N/A
Sv-04Ch19N11M3	10	3.8
Sv-08Ch19N10G2B	7	7.9

Table 4. The estimated and measured content of δ ferrite (%)

Material	$R_{p0.2}$ (MPa)	R_m (MPa)	A (%)
08Ch18N10T	286 ± 14	606 ± 10	41 ± 1
1.4541	305 ± 7	642 ± 3	49 ± 2
Sv-04Ch19N11M3	485 ± 10	620 ± 10	40 ± 3
Sv-08Ch19N10G2B	515 ± 5	690 ± 0	34 ± 1

Table 5. Mechanical properties of experimental alloys according to the inspection certificates

The tubes with an outside diameter of 32 mm (Fig. 1) were butt welded with a tungsten inert gas (TIG) 141-manual welding method in Argon 4.6 atmosphere. The WCe electrode with a diameter of 2.4 mm was used. Two passes filled the V-groove of 60°. The voltage 11 V, arc current 80 A, and welding speed 36 mm·min^{-1} were used for both root and filler (cover) passes in both samples, A and B. The welding parameters were chosen based on the certified Welding Procedure Qualification Record (WPQR). The short length of the available tube made of original steel allowed only one weld to be produced with each filler wire.

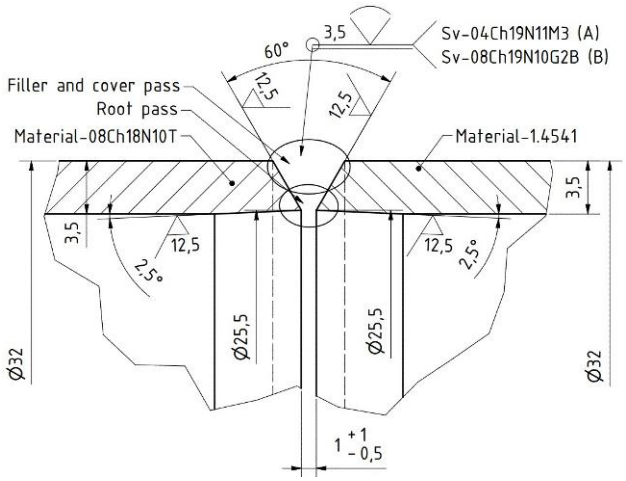

Figure 1. A detail of a weld

The visual and penetration tests were carried out after the welding. Then, the tubes were axially cut into two parts. The first part was used for the following tests.

The metallographic specimens of welds were prepared and etched with a solution of glycerin, hydrofluoric acid, and nitric acid (2:2:1) for 70 s to reveal weld macrostructure and grain boundaries. The WM microstructure was better revealed by electrolytic etching in a solution of 20 g of NaOH and 100 ml of distilled water at 3.5 V for 15 s. It was observed by laser scanning confocal microscope Keyence VK-X1000.

The scanning electron microscope (SEM) FEI Magellan 400 with AMETEK EDAX Hikari detector was used for electron backscatter diffraction (EBSD). The samples were electrolytically polished in Struers A2 at 25 V for 5 s. The EBSD data were collected at 20 keV landing energy of the primary electrons and beam current of 1.6 nA. The step size of 50 nm was utilized to obtain high-quality data.

The testing equipment type ZD 40 was used for tensile and bend tests at 20 °C according to EN ISO 4136 [CEN 2022] and EN ISO 5173 [CEN 2023], respectively. Due to the small diameter of a welded tube, only one test specimen of each weld could be examined in each test. Vickers microhardness test was performed with automatic hardness tester ATM CART 950 according to EN ISO 9015-2 [CEN 2016]. The 0.98 N load was applied for the indents distanced by 0.15 mm.

The NPPs of type WWER are assumed to have a service life of about 30–60 years. If the unit of NPP has an outage three times a year, there are about 150 thermal cycles in a whole service life. Therefore, 150 cycles were applied using the KSE 2x28/400-T furnace to simulate the cyclic aging of the second part of the welded tube. The samples were heated up from the initial temperature of 20–50 °C with a heating rate of 50 °C·h^{-1} until 300 °C was reached. The heating rate is 25 % increased towards the operating regulations and the peak temperature of 300 °C corresponds to the maximum work temperature of NPP units of type WWER (322 °C). After the dwell time of 10 minutes, the samples were spontaneously self-cooled in the furnace. The cooling time was about 18 hours. This thermal cycle was repeated 150 times. Then, the aged samples were subjected to the same tests as the as-welded samples, and the results were compared.

3 RESULTS

Based on nondestructive visual and penetration tests, the welds were acceptable and were further subjected to destructive tests.

3.1 Base metal microstructure

Fig. 2 shows the microstructures of BMs before and after the aging. The austenitic grains of the original BM are 10-35 µm in diameter. Comparable grain size was detected in substitutive steel. The outlined light-grey islands of δ ferrite are sporadic. The gold-etched polygonal particles are Ti(C,N). In the form of fine precipitates, they are dispersed within the austenitic grains and prevent the formation of chromium carbides, which would lead to a decrease in corrosion resistance. No significant changes observable by light microscopy were detected after the aging.

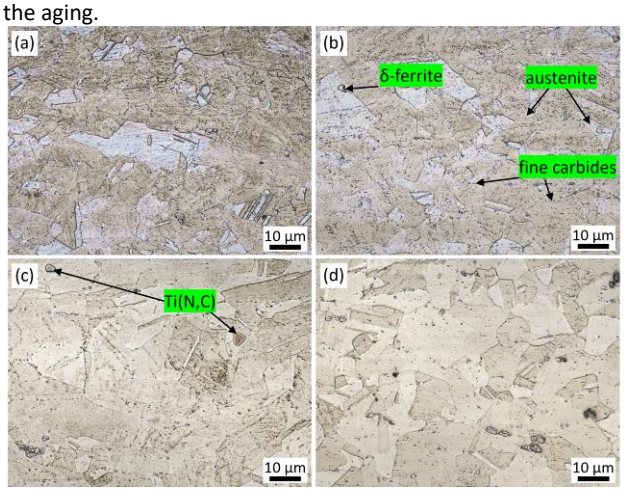

Figure 2. The microstructure of (a) substitutive steel 1.4541 and (b) original 08Ch18N10T steel. Images (c) and (d) show the corresponding steels after aging.

3.2 *Macro- and microstructure of welds*

Fig. 3 presents macrostructures of dissimilar welds. The substitutive steel 1.4541 is always on the left. The original 08Ch18N10T steel has a wider fusion line, representing a longer solidification time. Both welds were free of pores, cracks, or other unacceptable internal defects.

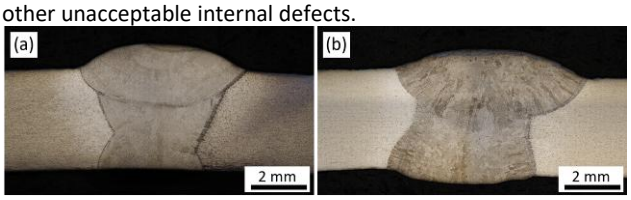

Figure 3. The macrostructure of as-welded (a) sample A and (b) sample B. The substitutive steel is on the left towards the weld metal.

The grain coarsening was observed in the HAZ of both alloys, similar for both samples. Fig. 4 presents the HAZs of sample A adjacent to the fusion zone in the middle of sheet thickness. The coarsening was higher in the case of substitutive 1.4541 steel (Fig. 4a,c). The largest grains reached a diameter of about 150 µm and 70 µm in substitutive and original steel, respectively. The aging vanished the deformation bands caused by the forming process and persisting in the HAZ after the welding. Nevertheless, it did not affect the grain size.

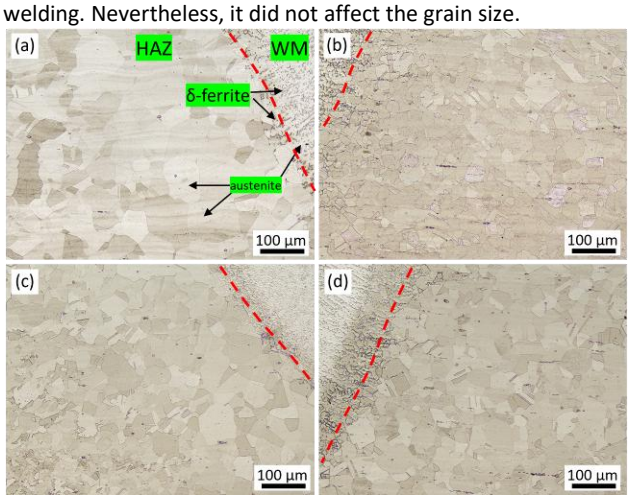

Figure 4. The heat-affected zone of sample A adjacent to the (a) 1.4541 and (b) 08Ch18N10T base metal in the as-welded condition. Images (c) and (d) show corresponding regions after aging. Red dashed curves assign the fusion lines.

Fig. 5 presents the dendritic microstructure of WMs detected in the middle of the cover beads. An austenitic matrix surrounds the ferritic islands. Based on the image analysis of three corresponding areas of each weld, 7–11 % of δ ferrite was found in sample A. The differences between the as-welded samples and the aged samples are lower than those detected within the one weld since the distribution of δ ferrite is not homogeneous. Sample B contained 7–13 % of δ ferrite, comparable to the sample A.

The EBSD analysis confirmed the presence of δ ferrite in the WM of the cover bead of all samples (Fig. 6). Its distribution is not homogeneous. To achieve a superior resolution the analyzed area was 35 µm × 26 µm. Therefore, the ferrite size and content differences between the as-welded and aged samples are caused by the measurement position rather than the effect of cyclic thermal loading.

Less than 0.5 % of the sub-micron σ phase was indexed in the WM of as-welded sample A randomly distributed in the ferritic islands (Fig. 6a). Nevertheless, this value is unconvincing and represents rather a measurement error. After the aging, no σ phase was detected either in sample A nor B.

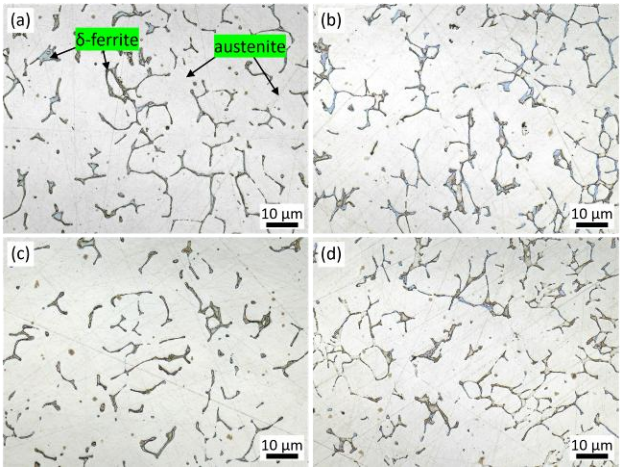

Figure 5. Microstructure of weld metal in the as-welded condition for (a) sample A and (b) sample B. Images (c) and (d) show corresponding regions after aging.

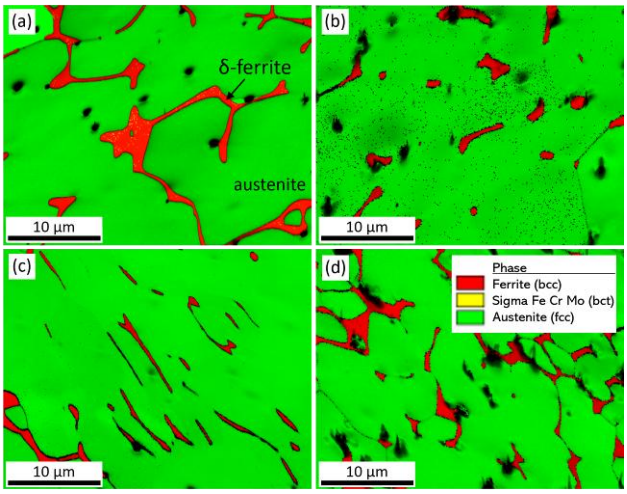

Figure 6. The EBSD phase + image quality maps of the weld metal in the as-welded condition for (a) sample A and (b) sample B. Images (c) and (d) show corresponding regions after aging. The legend is the same for all images.

3.3 *Mechanical properties of welds*

All specimens withstood the bend test and did not report any defects at the bend angle of 180°. The thermal loading did not affect the weld deformation ability.

All specimens fractured in the WM during the static tensile test (Fig. 7). The as-welded samples A and B reached the UTS of 525 MPa and 562 MPa, respectively. The higher UTS of sample B corresponds to the higher carbon content in the filler.

The thermal loading increased the UTS of welds A and B to 589 MPa and 584 MPa, respectively. These values are less than 4% lower than the original 08Ch18N10T steel (Tab. 5) and fulfill the minimum required value of 550 MPa.

Figure 7. Fractured tensile specimens of (a) sample A and (b) sample B in the as-welded condition. Images (c) and (d) show corresponding specimens of aged welds.

The average microhardness of BM 1.4541 and 08Ch18N10T was (190 ± 10) HV 0.1 and (187 ± 8) HV 0.1, respectively. Fig. 8 presents the maps of microhardness measured across both welds. The as-welded sample A reached the average WM microhardness (164 ± 11) HV 0.1, about 12 % lower than the 08Ch18N10T BM. The average WM microhardness of sample B was (163 ± 12) HV 0.1, i.e., the same as for sample A.

The cyclic thermal loading did not affect the BMs. The changes in microhardness were -2 %, thus lower than the standard deviations calculated for the BMs in default condition. Similarly, the average microhardness of WM of sample A did not change by thermal loading, and that of sample B increased by 8 %.

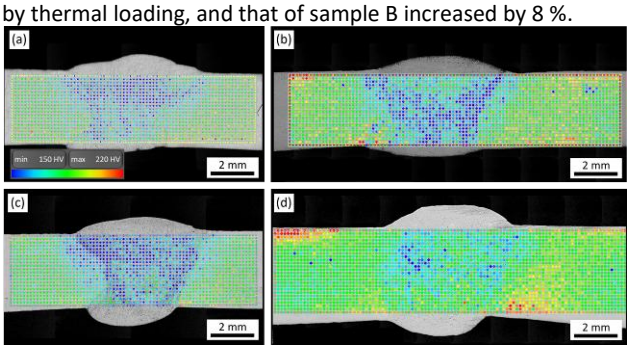

Figure 8. Vickers microhardness of (a) sample A and (b) sample B in the as-welded condition. Images (c) and (d) show the microhardness of corresponding specimens after aging. The legend is the same for all images.

4 DISCUSSION

Both BMs belong to the group 8.1 according to the ISO/TR 15608 [ISO 2017]. Thus, they should have excellent weldability with any welding technology adequately protecting the melt pool. The TIG dissimilar welds did not exhibit any pores, cracks, or other unacceptable internal defects. The substitutive steel experienced twice as high grain coarsening in the HAZ, originating from the absence of vanadium and nitrogen that would form the precipitates, limiting the grain growth. According to the Hall-Petch formula, the higher the degree of grain coarsening in the HAZ, the lower yield strength could be expected in this region. However, samples with welds (moreover dissimilar welds) are highly heterogeneous. Thus, their yield strength cannot be reliably evaluated. The grain coarsening did not have a negative effect on tensile strength since all the samples fractured in the softer WM. The grain coarsening neither changed during the thermal cycling. All specimens also withstood the bend test and did not report any defects at the bend angle of 180°. The cyclic thermal loading did not affect the weld deformation ability.

Both welds had a comparable portion of δ ferrite of about 10 %. It was nonhomogeneously distributed in the WM. Such value corresponds to the predictions of the Schaeffler diagram, assuming at least 60 % of the filler material in the WM. The content of δ ferrite would decrease with increasing level of dilution. The cyclic thermal loading had no measurable effect on the δ ferrite content. Less than 0.5 % of the sub-micron σ phase was indexed in the WM of as-welded sample A randomly distributed in the ferritic islands (Fig. 6a). Nevertheless, this is more like a measurement error, also supported by the fact that no σ phase was detected in thermally loaded welds. However, the randomly distributed phases of sub-micron size are challenging for SEM to detect when relatively large areas have to be analyzed.

At comparable content of C and Cr, the substitutive steel has a lower portion of austenite-stabilizing Ni [Steiner 2005] than the original steel (Tab. 3). Therefore, the WM of dissimilar weld between the original and substitutive steel was supposed to have a higher ratio factor at the same level of dilution and thus the higher risk of σ phase formation compared to the homogeneous weld of original steel. Nevertheless, neither the welding nor the applied heat treatment simulating real operating conditions did not allow the σ phase precipitation.

Although no σ phase was found in the WM of both aged samples, their UTS increased towards the as-welded. The higher strengthening (12 %) was detected in weld A made with Sv-04Ch19N11M3 filler containing a lower portion of δ ferrite in the as-welded condition. However, the microhardness of this weld remained constant. Weld B experienced an 8% increase in WM microhardness. Such change is quite unconvincing, considering the 5–7% standard deviations of each sample measurement. However, it can indicate precipitation of the G phase accompanied by ferrite microhardness increase [Liu 2022, Raj 2024]. Ferrite decomposition reduces weld fracture resistance synergically with neutron irradiation [Kim 2024]. Fekete et al. [Fekete 2015] reported hardening and a decrease in 08Ch18N10T steel fatigue life of thermomechanically loaded specimens towards those subjected to the isothermal low-cycle fatigue tests. The welds of this steel have lower fatigue strength at increased temperatures than the base metal [Timofeev 2007]. The welds of another austenitic grade also report worse very high cycle fatigue properties at increased temperatures compared to the ambient [Smaga 2024]. Thus, the dissimilar welds need to be further examined from this point of view.

The UTS of both welds after the aging was less than 4 % lower than the original 08Ch18N10T BM. Both fulfilled the minimal required value of 550 MPa. Nevertheless, the number of specimens for mechanical tests was very limited because of the short length of the available tube made of original steel. Therefore, no definite conclusions concerning tensile properties can be stated, and further research must be done. However, a current shortage of the original steel is a limiting factor.

It is also necessary to point out that the WM was dominantly formed by the filler wire relatively little diluted with BMs. Thus, the effect of substitutive steel in the dissimilar weld was suppressed. According to the inspection certificates (Tab. 5), the fillers should have the UTS higher than the original steel. However, in our experiments, the tensile specimens always fractured in the WM at 5–15 % lower UTSs than declared. In the future, it will be necessary to replace not only the material of a tube but also the fillers. The filler wire composition and adequate heat input are crucial for weld joint properties.

5 CONCLUSIONS

The dissimilar welds of original Russian steel 08Ch18N10T and substitutive 1.4541 were analyzed to consider the possibility of original steel replacement during repairing parts of NPPs repeatedly exposed to the increased temperatures of 300 °C. The two different filler wires were used. Both welds contained about 10 % of δ ferrite in the austenitic WM in as-welded condition. After the cyclic thermal aging with a total exposure of welds to the peak temperatures of 300 °C for about 25 h, no changes in ferrite content were detectable with optical microscopy. However, the WM microhardness of the weld made with a filler with higher C and Cr content increased by 8 % at an insignificant 4% increase in the UTS, still matching the requirements for the steel used in NPP devices. This could

indicate the ferrite decomposition. The filler wire with a lower C and Cr content would be safer since no negative microhardness changes caused by the aging were detected.

Based on our preliminary tests, the substitutive steel seems to be applicable with so far used filler wires for the repair welds because the changes induced by cyclic thermal loading in heterogeneous welds were comparable to the changes induced by continuous thermal aging of homogeneous welds of original steel summarized in [Kazantsev 2009]. Nevertheless, further research is required to analyze weld toughness to ensure the safe and long-lasting operation of NPPs.

ACKNOWLEDGMENTS

The research infrastructure was funded by the Czech Academy of Sciences (RVO:68081731).

REFERENCES

[Brandi 2017] Brandi, S.D. and Schön, C. G. A Thermodynamic Study of a Constitutional Diagram for Duplex Stainless Steels. Journal of Phase Equilibria and Diffusion, 2017, Vol. 38, No. 3, pp 268–275. doi: 10.1007/s11669-017-0537-8.

[CEN 2016] European Committee for Standardization. Destructive tests on welds in metallic materials — Hardness testing — Part 2: Microhardness testing of welded joints. EN ISO 9015-2:2016. Brussels: European Committee for Standardization, 2016, p. 15.

[CEN 2022] European Committee for Standardization. Destructive Tests on Welds in Metallic Materials — Transverse Tensile Test. ISO 4136:2022, Brussels: European Committee for Standardization, 2022; p. 17.

[CEN 2023] European Committee for Standardization. Destructive tests on welds in metallic materials — Bend tests. ISO 5173:2023. Brussels: European Committee for Standardization, 2023; p. 31.

[Chandra 2012] Chandra, K. et al. Low temperature thermal aging of austenitic stainless steel welds: Kinetics and effects on mechanical properties. Materials Science and Engineering A, 2012, Vol. 534, pp 163–175. doi: 10.1016/j.msea.2011.11.055.

[Chen 2002] Chen, T. H. et al. The effect of high-temperature exposure on the microstructural stability and toughness property in a 2205 duplex stainless steel. Material Science and Engineering A, 2002, Vol. 338, No. 1–2, pp 259–270. doi: 10.1016/S0921-5093(02)00093-X.

[Dutt 2011] Dutt, B. S. et al. Mechanical behaviour of SS 316 (N) weld after long term exposure to service temperatures. Procedia Engineering, 2011, Vol. 10, pp 2725–2730. doi: 10.1016/j.proeng.2011.04.454.

[Eghlimi 2015] Eghlimi, A. et al. Characterization of microstructure and texture across dissimilar super duplex/austenitic stainless steel weldment joint by super duplex filler metal. Materials Characterization, 2015, Vol. 106, pp 27–35. doi: 10.1016/j.matchar.2015.05.017.

[Energoatomizdat 1987] Energoatomizdat. PNAE G-7-002-86 Rules of strength calculation for equipment and pipelines of nuclear power plants. Moscow: Energoatomizdat, 1987, p. 499.

[Fekete 2015] Fekete, B. et al. Low cycle thermomechanical fatigue of reactor steels: Microstructural and fractographic investigations. Materials Science & Engineering A, 2015, Vol. 640, pp 357–374. doi: 10.1016/j.msea.2015.05.093.

[Fujiyama 2018] Fujiyama, N. and Seki, A. Austenite grain growth simulation in welding heat-affected zone. Materials Science Forum, 2018, Vol. 941, No. 119, pp 620–626. doi: 10.4028/www.scientific.net/MSF.941.620.

[GOST 2014] Russian GOST. Stainless steels and corrosion resisting, heat-resisting and creep resisting alloys. Grades. GOST 5632-2014. Russian GOST, 2014 (in Russian).

[Gow 1942] Gow, J. T. and Harder, O. E. Balancing the Composition of Cast 25 per Cent Chromium-12 per Cent Nickel Type Alloys. Transactions of American Society for Metals, 1942, Vol. 30, pp 855–935.

[Hsieh 2012] Hsieh, C.-C. and Wu, W. Overview of Intermetallic Sigma (σ) Phase Precipitation in Stainless Steels. ISRN Metallurgy, 2012, Vol. 2012, No. 4, pp 1–16. doi: 10.5402/2012/732471.

[ISO 2017] International Organization for Standardization. Welding — Guidelines for a metallic materials grouping system. ISO/TR 15608:2017, Geneva: International Organization for Standardization, 2017; p. 9.

[Jeong 2022] Jeong, C. et al. Evaluation of thermal aging activation energies based on multi-scale mechanical property tests for an austenitic stainless steel weld beads. Materials Science and Engineering A, 2022, Vol. 835, pp 142629. doi: 10.1016/j.msea.2022.142629.

[Kander 2023] Kander, L. Normative technical documentation of the Association of Mechanical Engineers – Section II. Association of Mechanical Engineers, 2023.

[Kazantsev 2009] Kazantsev, G. et al. Prediction of mechanical properties and crack resistance characteristics of metal of pipelines from corrosion-resistant steels to substantiate service life extension of NPPs with WWER. Moscow: JSC NPO Cniitmash & Podolsk: OKB Gidropress, 2009, p. 23 (in Russia).

[Kim 2024] Kim, J.-S. and Kim, J.-M. Mechanical characterization of synergistic thermal and irradiation effects on fracture resistance of stainless steel. International Journal of Mechanical Sciences, 2024, Vol. 281, pp 109567. doi: 10.1016/j.ijmecsci.2024.109567.

[Klimpel 2007] Klimpel, A. and Lisiecki, A. Laser welding of butt joints of austenitic stainless steel AISI 321. Journal of Achievements in Materials and Manufacturing Engineering, 2007, Vol. 25, No. 1, pp 63–66.

[Kumar 2021] Kumar, T. S. et al. Deformation and failure behaviour of 316 LN austenitic stainless steel weld joint under thermomechanical low cycle fatigue in as-welded and thermally aged conditions. International Journal of Fatigue, 2021, Vol. 149, pp 106269. doi: 10.1016/j.ijfatigue.2021.106269.

[Lapsanska 2010] Lapsanska, H. et al. Effect of beam energy on weld geometric characteristics in Nd:YAG laser overlapping spot welding of thin AISI 304 stainless steel sheets. Metallurgical and Materials Transactions B, 2010, Vol. 41, No. 5, pp 1108–1115. doi: 10.1007/s11663-010-9399-8.

[Lee 2003] Lee, J. et al. Application of small punch test to evaluate sigma-phase embrittlement of pressure vessel cladding material. Journal of Nuclear Science

and Technology, 2003, Vol. 40, No. 9, pp 664–671. doi: 10.1080/18811248.2003.9715404.

[Liu 2022] Liu, X. et al. Mediating phase decomposition to avoid thermal aging embrittlement in a duplex stainless steel. Materials Characterization, 2022, Vol. 194, pp 112411. doi: 10.1016/j.matchar.2022.112411.

[Nagae 2022] Nagae, K. et al. Effect of Sigma Phase on Corrosion Behavior of Duplex Stainless Steel. Materials Transactions, 2022, Vol. 63, No. 5, pp 726–729. doi: 10.2320/matertrans.MT-MA2022002.

[Peckner 1977] Peckner, D. and Bernstein, I. M. Handbook of Stainless Steels, 1st ed., New York: McGraw-Hill, 1977.

[Raj 2024] Raj, C. R. et al. Thermal aging effects on Tensile and Metallurgical characteristics of Stainless steel weld joint. Procedia Structural Integrity, 2023, Vol. 60, pp 709–722. doi: 10.1016/j.prostr.2024.05.088.

[Smaga 2024] Smaga, M. et al. Very high cycle fatigue of austenitc stainless steels and their welds for reactor internals at ambient temperature and 300 °C. International Journal of Pressure Vessels and Piping, 2024, Vol. 212, Part A, pp 105319. doi: 10.1016/j.ijpvp.2024.105319.

[Steiner 2005] Steiner, R. Sigma phase embrittlement, in ASM Handbook, Volume 1, Properties and Selection: Irons, Steels, and High Performance Alloys, ASM International, 2005; p. 1618.

[Subramanian 2018] Subramanian, G. O. et al. Evaluation of the thermal aging of δ-ferrite in austenitic stainless steel welds by electrochemical analysis. Scientific Reports, 2018, Vol. 8, No. 1, pp 1–17. doi: 10.1038/s41598-018-33422-x.

[Timofeev 2007] Timofeev, B. T. and Bazaras, Zh. L. Low-cycle fatigue of welded joints of 08Kh18N10T steel. Materials Science, 2007, Vol. 43, No. 1, pp 117–123. doi: 10.1007/s11003-007-0013-4.

[Wang 2022] Wang, Q. et al. Role of δ-ferrite in fatigue crack growth of AISI 316 austenitic stainless steel. J. Materials Science Technology, 2022, Vol. 114, pp 7–15. doi: 10.1016/j.jmst.2021.10.008.

CONTACTS:

Hana Sebestova, Ph.D.
Institute of Scientific Instruments of the CAS
Department of Coherence Optics
Kralovopolska 147, Brno 612 00, Czech Republic
sebestova@isibrno.cz